How well can we measure the ocean's mean dynamic topography from space?

AGU PUBLICATIONS

JGR

Journal of Geophysical Research: Oceans

RESEARCH ARTICLE

10.1002/2013JC009354

How well can we measure the ocean's mean dynamic topography from space?

R. J. Bingham[1], K. Haines[2], and D. J. Lea[3]

[1]School of Geographical Sciences, University of Bristol, Bristol, UK, [2]Department of Meteorology, University of Reading, Reading, UK, [3]Met Office, Exeter, UK

Key Points:
- Geodetic MDT errors can be accounted for in terms of MSS and geoid errors
- Geoid (MSS) errors dominate for spatial scales less (greater) than about 250 km
- In situ data do not restore all the signal lost when a geodetic MDT is filtered

Correspondence to:
R. J. Bingham,
rory.bingham@bristol.ac.uk

Citation:
Bingham, R. J., K. Haines, and D. J. Lea (2014), How well can we measure the ocean's mean dynamic topography from space?, *J. Geophys. Res. Oceans*, *119*, 3336–3356, doi:10.1002/2013JC009354.

Received 14 AUG 2013
Accepted 15 MAY 2014
Accepted article online 21 MAY 2014
Published online 4 JUN 2014

Abstract Recent gravity missions have produced a dramatic improvement in our ability to measure the ocean's mean dynamic topography (MDT) from space. To fully exploit this oceanic observation, however, we must quantify its error. To establish a baseline, we first assess the error budget for an MDT calculated using a 3rd generation GOCE geoid and the CLS01 mean sea surface (MSS). With these products, we can resolve MDT spatial scales down to 250 km with an accuracy of 1.7 cm, with the MSS and geoid making similar contributions to the total error. For spatial scales within the range 133–250 km the error is 3.0 cm, with the geoid making the greatest contribution. For the smallest resolvable spatial scales (80–133 km) the total error is 16.4 cm, with geoid error accounting for almost all of this. Relative to this baseline, the most recent versions of the geoid and MSS fields reduce the long and short-wavelength errors by 0.9 and 3.2 cm, respectively, but they have little impact in the medium-wavelength band. The newer MSS is responsible for most of the long-wavelength improvement, while for the short-wavelength component it is the geoid. We find that while the formal geoid errors have reasonable global mean values they fail capture the regional variations in error magnitude, which depend on the steepness of the sea floor topography.

1. Introduction

If the ocean were at rest, its surface would coincide with the particular equipotential surface of earth's gravity field known as the geoid. The ocean's mean dynamic topography (MDT) is the deviation of the time-mean sea surface (MSS) from this rest position. This relationship has the elementary mathematical expression $\eta = H - N$, where $\eta(\lambda, \theta)$ is the MDT, $H(\lambda, \theta)$ and $N(\lambda, \theta)$ are the heights of the MSS and geoid above a common reference ellipsoid, and λ and θ are longitude and latitude. The MDT is primarily of interest to oceanographers because it can be used to calculate the ocean's surface geostrophic circulation. Alternatively, an MDT estimate may be used directly to constrain an ocean model [e.g., *Drecourt et al*., 2006; *Lea et al*., 2008; *Haines et al*., 2011], and also has applications beyond oceanography, such as in the determination of vertical datums [e.g., *Featherstone and Filmer*, 2012; *Woodworth et al*., 2013].

It is possible to measure the MDT using satellite observations of earth's gravity field and the ocean's surface. The advantage of this geodetic approach is that it can be used to determine a global MDT with relatively homogeneous error characteristics. However, to measure the ocean's MDT with sufficient resolution and accuracy to improve upon what can be achieved using in situ observations, both the gravity field and the MSS must be measured to a high degree of accuracy. This stringent requirement hampered early attempts to measure the MDT from space [e.g., *Tai and Wunsch*, 1983; *Denker and Rapp*, 1990; *Nerem et al*., 1990], with the poor accuracy of the first global gravity models being the limiting factor.

However, the Gravity Recovery And Climate Experiment (GRACE) satellite mission, launched in 2002, produced a step change in our ability to measure earth's global gravity field from space. This, together with concomitant progress in satellite altimetry, lead to oceanographically informative estimates of the ocean's MDT determined using only satellite observations [e.g., *Jayne et al*., 2003; *Tapley et al*., 2003].

Despite this progress, it is evident from in situ drifter observations [e.g., *Niiler et al*., 2003] that the ocean's MDT contains finer scales than can be resolved by GRACE. Consequently, the Gravity and steady state Ocean Circulation Explorer (GOCE) satellite was launched by ESA in March 2009. Flying at an altitude of 250 km—extremely low for an earth observation satellite—and carrying a three-axis gradiometer, GOCE was specifically designed to measure the small spatial scales (100–200 km) of earth's gravity that are not well resolved

by GRACE. As such, GOCE has allowed the ocean's mean circulation to be mapped globally in unprecedented detail from space [e.g., *Bingham et al*., 2011; *Knudsen et al*., 2011; *Volkov and Zlotnicki*, 2012].

Although GOCE has improved the resolution of the geodetic approach, GOCE MDTs still contain noise that must be removed by filtering. To do this rigorously we must quantify the MDT error. An error estimate is also required if an MDT is to be used to constrain an ocean model. Estimating MDT error, however, is not straightforward. One simple approach, is to compare the spread of a range of MDTs. Using such a method, *Vossepoel* [2007] found the pre-GOCE uncertainty on observational MDTs to be 10 cm at spatial resolutions of 170 km. Alternatively, in the context of finding optimum filter characteristics, some recent studies have employed heuristic strategies to estimate MDT noise [*Bingham et al*., 2011; *Knudsen et al*., 2011]. While such methods have the advantage of being relatively easy to compute, given that there must also be errors in the external reference surfaces they use, it is not clear how representative they will be of the actual MDT error.

A novel feature of the GOCE mission is the provision of the full error variance-covariance matrix associated with each GOCE gravity model. Potentially, this allows a robust estimate of MDT error across all resolved scales to be determined. Yet there are a number of confounding factors to consider: First, due to the nature of their calculation, and the fact that systematic errors cannot be accounted for, it cannot be taken for granted that formal errors are an accurate estimate of the true geoid commission error; A point noted by *Wunsch and Gaposchkin* [1980]. Second, the formal geoid error does not include geoid omission error (that part of the gravity field not resolved by the model), or numerical errors resulting from the process of truncating the spherical harmonic series representing the gravity field [*Bingham et al*., 2008]. Third, we must also consider the MSS contribution to the MDT error budget.

Our objective in this paper is to bring together evidence from a number of independent sources to give a robust estimate of the error for an MDT obtained from a GOCE geoid and an altimetric MSS. Furthermore, we examine how this error depends on spatial scale and we assess the relative contributions of the geoid and MSS to the MDT error budget.

The remainder of the paper is structured as follows: In section 2 we describe the calculation of our baseline MDT, which we shall refer to as BHL14. Then, in section 3, we derive informal error estimates for BHL14, and the geoid and MSS from which it is calculated. In section 4 we compare the informal error estimates for the GOCE geoid and the MSS with their formal errors. Having established the error characteristic of the baseline MDT, in section 5 we consider the extent to which the most recent geoid and MSS products can improve upon BHL14. A concluding discussion is provided in section 6.

2. The BHL14 MDT

The BHL14 MDT is calculated using a gravity model provided by the GOCE High-level Processing Facility. Within this facility three processing strategies have been adopted, each with a distinct approach to generating the gravity model from the basic satellite-to-satellite tracking and gradiometer observations. An overview is provided by *Pail et al*. [2010a]. We use the third generation gravity model obtained by the so-called timewise approach (henceforth GTIM3) using 1 year of GOCE observations covering the period November 2009 to April 2011. Uniquely, the timewise approach is based purely on observations from GOCE.

The GTIM3 geoid is subtracted from the CLS01 MSS [*Hernandez and Schaeffer*, 2001]. This surface corresponds to the 1993–1999 time-mean period and is derived from 7 years of Topex/Poseidon data, 5 years of ERS-1/2 repeat-track and geodetic data, and 2 years of GEOSAT data. It is defined globally between 80° S and 82° N, on a regular grid with a spatial resolution of 2 arc-minutes, based on the nonrepeating geodetic sampling of the ERS and GEOSAT missions.

CLS01 and GTIM3 are not the most recent products available. However, they provide a baseline geodetic MDT against which improvements delivered by more recent products can be assessed. We therefore consider the extent to which the more recent 4th generation timewise solution (GTIM4), based on 26 months of observations, and the CLS11 MSS [*Schaeffer et al*., 2012], which is calculated from observations gathered over 15 years, improve upon BHL14.

The BHL14 MDT is computed on a global $0.5^\circ \times 0.5^\circ$ grid (used as the common grid for all comparisons in this study) by the spectral method as described in *Bingham et al*. [2008] whereby the MSS is first

represented as a set of spherical harmonic coefficients. This allows the MDT to be computed up to a given harmonic degree L: $\eta_L = H_L - N_L$ (where the spatial resolution of η_L is $\sim$20,000/L km). Increasing L may improve MDT resolution, sharpening gradients and resolving finer scale features of the ocean's circulation. However, errors in the MSS and especially in the geoid also grow with increasing L, potentially outweighing any benefit from reduced MDT omission error.

To illustrate this issue, Figure 1 presents three versions of the BHL14 MDT, increasing in resolution from $L=80 \approx 250$ km , to $L=150 \approx 133$ km , and finally to $L=250 \approx 80$ km (the maximum degree and order of the GTIM3 model). The enhancement of gradients associated with strong currents such as the Gulf Stream, Agulhas retroflection and the Antarctic Circumpolar Current (ACC) can be seen as the resolution is increased from 250 to 133 km. This gain is seen more clearly in the increment defined by the spherical harmonic coefficients of degree $l=81,\ldots,150$ (Figure 1d), which we shall refer to as the medium-wavelength MDT component, with the $L = 80$ MDT corresponding to the long-wavelength component. Further, though diminishing, gains may be expected as the resolution is increased from 133 to 80 km. However, the level of noise has now markedly increased (Figure 1c). Again, this is seen most clearly in the increment defined by the spherical harmonic coefficients of degree $l=151,\ldots,250$ (Figure 1e), which we shall refer to as the short-wavelength MDT component.

A first impression of the likely error in BHL14 can be obtained simply by comparing its RMS amplitude with that from a range of independent MDTs (these reference MDTs are described in Appendix A; the RMS amplitude is computed in a $10^\circ \times 10^\circ$ window around each grid point). For long-wavelengths, there is close agreement between BHL14 and the CLS09 and MAX11 reference MDTs, both of which use a GRACE-based geodetic MDT as the first guess (Figure 2a). In contrast, for the medium-wavelength component BHL14 clearly emerges as an outlier, suggesting the growth of errors in our MDT (Figure 2b). The difference between BHL14 and the reference MDTs is even more pronounced for the short-wavelength component (Figure 2c), confirming the visual impression of Figure 1e that short-wavelength errors are much larger than any residual signal.

Quantifying this growth in error is an essential first step toward extracting the greatest advantage from geodetic MDTs, and is the primary objective of the remainder of this paper.

3. Informal Error Estimates

The basis of our informal approach to estimating errors is quite simple: using available reference surfaces, we compute, for each wavelength band, a set of RMS differences for BHL14 and corresponding sets for its constituent surfaces—the GTIM3 geoid and the CLS01 MSS. (The reference surfaces and the calculation of the RMS differences are described in Appendix A.) To distinguish them from the formal error estimates for GTIM3 and CLS01 to be discussed later, we shall refer to these RMS differences as *informal* error estimates.

For each wavelength band, we use three reference MDTs to compute three BHL14 error estimates. Additionally, we form a further three estimates by computing the mean of each pair of RMS differences and a further estimate from the mean of all three RMS differences, giving a set of informal BHL14 error estimates $\epsilon_i^\eta, i=1,\ldots,7$. Similarly, from a set of three independent gravity fields (that do not include GOCE data) we calculate a set of informal GTIM3 geoid error estimates $\epsilon_j^N, j=1,\ldots,7$ for each wavelength band. Likewise, from two reference mean sea surfaces we calculate a set of informal CLS01 MSS error estimates $\epsilon_k^H, k=1,\ldots,3$.

From these three sets, representing 147 possible combinations, we select the three "best" BHL14, CLS01 and GTIM3 error estimates ϵ^η, ϵ^H and ϵ^N as those that minimize $<\epsilon^\eta - E^\eta>$ where

$$E^\eta = \sqrt{(\epsilon^H)^2 + (\epsilon^N)^2} \tag{1}$$

is a second error estimate for BHL14 assuming the GTIM3 and CLS01 errors are independent, and where $<*>$ represents the global RMS of quantity *.

The assumption of independence was tested by allowing the error correlation parameter c to vary between -1 and 1 in the full error propagation expression for the difference between two measurements

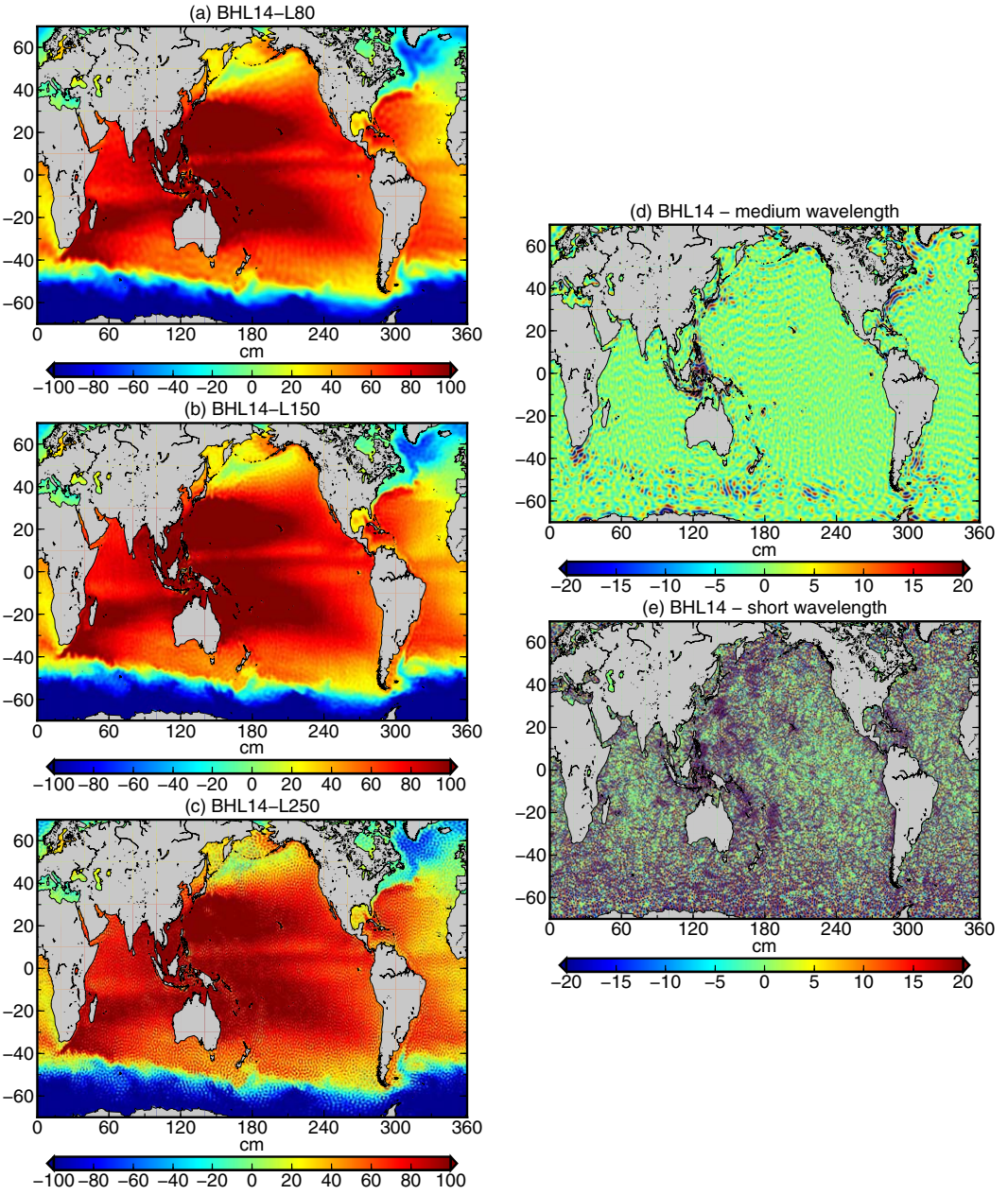

Figure 1. The BHL14 MDT calculated from the CLS01 MSS and the third generation GOCE time-wise (GTIM3) gravity model. BHL14 is shown truncated at degree and order (a) $L = 80$ (the long-wavelength component of BHL14), (b) $L = 150$ and (c) $L = 250$. (d) The medium-wavelength component of BHL14 obtained by subtracting the $L = 80$ version from the $L = 150$ version. (e) The short-wavelength component of BHL14 obtained by subtracting the $L = 150$ version from the $L = 250$ version.

$$E^{\eta} = \sqrt{(\epsilon^H)^2 + (\epsilon^N)^2 - 2c\epsilon^H\epsilon^N} \tag{2}$$

when searching for the minimizing combination. For the short-wavelength component, $c_{min} = 0$, and for the medium wavelength component $c_{min} = -0.2$, which had little impact on E^{η}. For the long-wavelength component, $c_{min} = -1.0$. But, given there is no good reason why the geoid and MSS errors should be perfectly anticorrelated, this just reflects the fact that there is a large discrepancy between the two long-wavelength MDT error estimates which can be reduced (by 3 mm RMS) by adding the errors rather than summing them in quadrature. The change in E^{η} obtained by using a more plausible, but arbitrary, value of

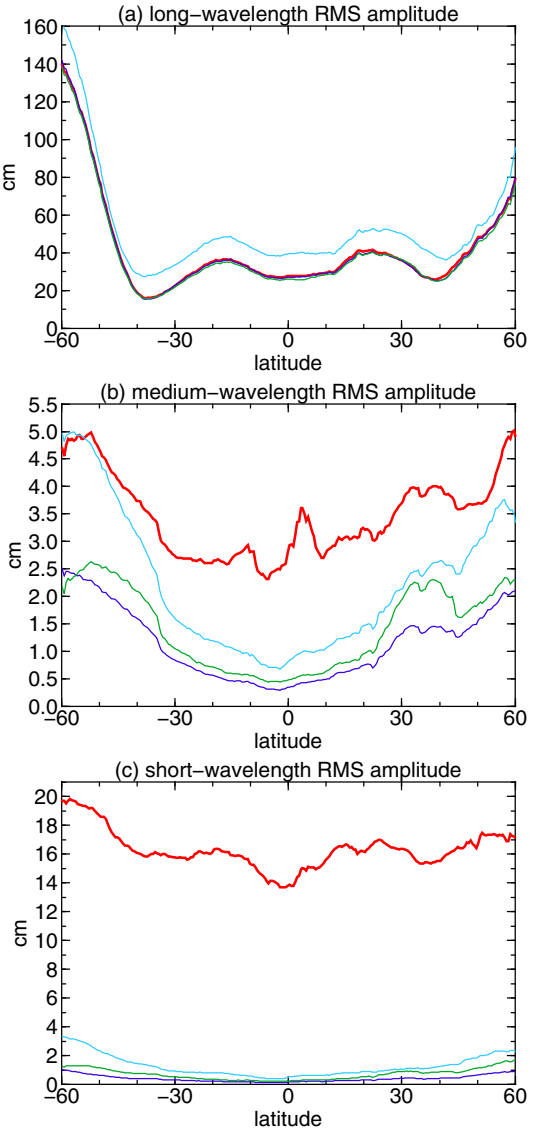

Figure 2. A comparison of the RMS amplitude for the (a) long, (b) medium, and (c) short-wavelength components of the BHL14 MDT (red) and the CLS09 (green), MAX11 (blue) and NLR03 (cyan) reference MDTs.

−0.5 has a negligible impact on the analysis as presented below. Therefore, we proceed with the assumption that the geoid and MSS errors are independent.

3.1. Long-Wavelength Errors

Errors in the long-wavelength component of BHL14 are the most difficult to determine. This is because the amplitude of the signal is much greater than that of the error. Comparing the maps of ϵ^{η} and E^{η} (Figures 3a and 3b) we see that the error estimate based on the comparison with other MDTs gives much larger values over much of the Southern Ocean, around the Caribbean, along the path of the Gulf Stream and in the subpolar gyres of the North Atlantic and North Pacific; all regions of strong currents and steep MDT gradients. For these regions the difference between ϵ^{η} and E^{η} can exceed 6 cm (Figure 3c). We also see from Figure 3c that ϵ^{η} is greater than E^{η} by around 1–2 cm even in regions away from strong currents. This difference is seen clearly in the zonal and meridional means of the two error estimates (see Figures 4a and 4b), and in their global mean values (3.9 cm for ϵ^{η} and 1.7 cm for E^{η}). The aforementioned regional differences manifest themselves as the divergence of the zonal mean error estimates toward higher latitudes and the three peaks in the meridional mean error estimate seen in ϵ^{η} but not in E^{η}.

For long-wavelengths, ϵ^{η} is given by the mean of the RMS differences calculated using the CLS09 and MAX11 MDTs, both of which use a GRACE-based geodetic MDT as their foundation, leaving the NLR03 based error estimates as outliers. Long-wavelength errors in NLR03 are to be expected given that gravity data are not used in its calculation. In fact, in Figures 4a and 4b we have not shown the informal estimates incorporating the NLR03-based RMS differences as these are several times greater than the other RMS differences. (Note, since it is dynamically inconsequential, any nonzero global mean is removed from the MDTs prior to our analysis.)

Are the substantial long-wavelength differences between BHL14 and the reference MDTs seen in regions of strong currents the result of errors in BHL14? If this were so, then the fact that such errors are not seen in E^{η} would imply that either the set of geoids or the set of mean sea surfaces used in this analysis are biased in these regions. This is improbable, particularly given that the long-wavelength components of the reference MDTs come from GRACE-based geodetic MDTs. A simple comparison of the long-wavelength components

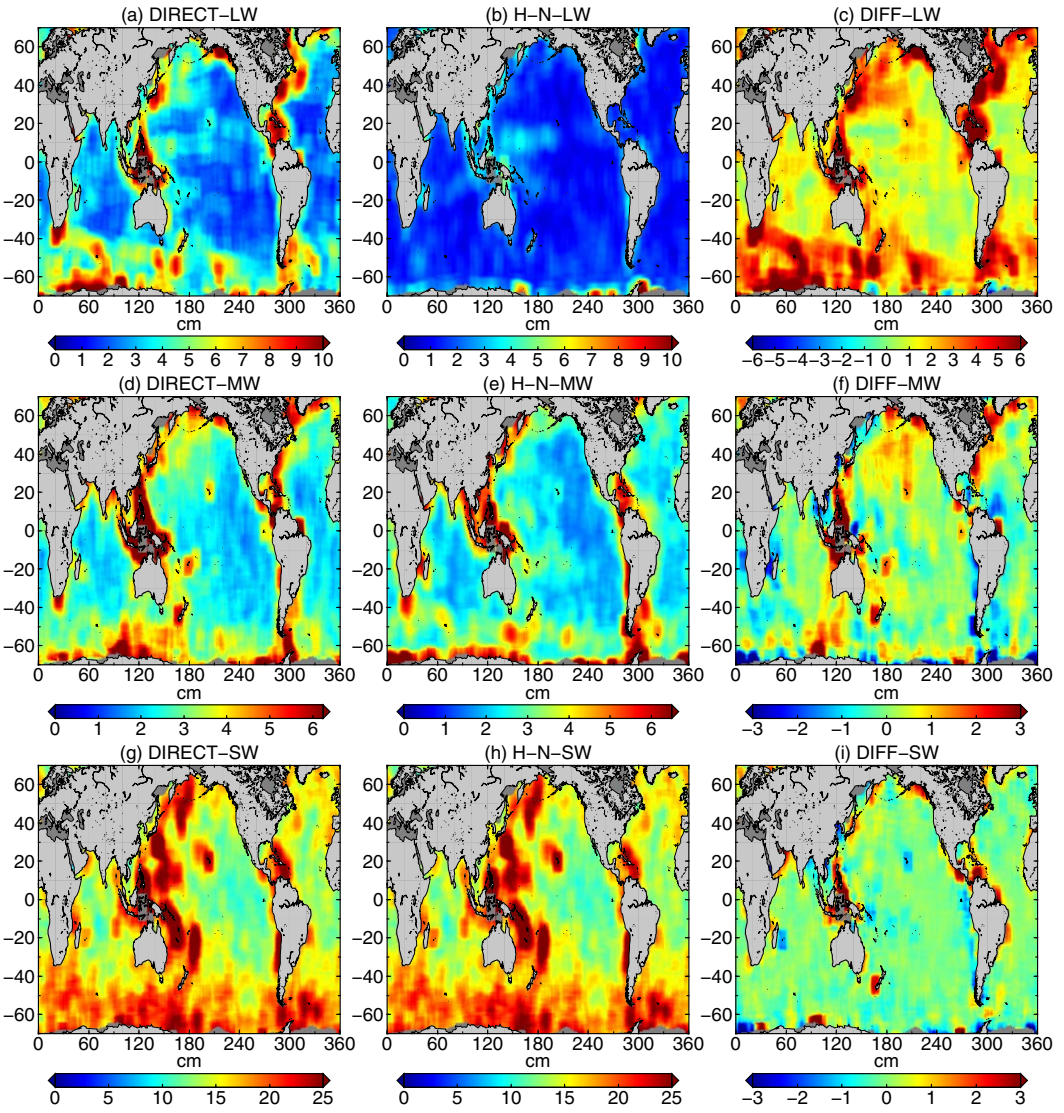

Figure 3. (a) The direct informal error estimate for the long-wavelength component of BHL14. (b) The BHL14 long-wavelength error from the quadratic sum of the informal GTIM3 and CLS01 errors. (c) The direct minus the quadratic sum estimates of the long-wavelength BHL14 error. (d-f) Repeating Figures 3a–3c for the medium-wavelength component of BHL14. (g-i) Repeating Figures 3a–3c for the short-wavelength component of BHL14.

of BHL14 and CLS09 over the northern hemisphere oceans (Figure 5) reveals that the long-wavelength component of CLS09 has generally weaker gradients than those of BHL14. The subpolar gyres, both of which are much better defined in BHL14, are clear examples of this. The gradients associated with the northern equatorial currents are also weaker in CLS09. This relative weakness is also a feature of the MAX11 MDT (not shown).

However, it is also clear from (Figure 5) that the long-wavelength component of BHL14 contains smaller scale eddy-like features not present in the smoother CLS09 MDT. It is these features that lead to the overall 1–2 cm larger error estimate given by ϵ^{η}. It seems likely these smaller scale features of BHL14 are noise, rather than realistic features of the ocean circulation lost when the geodetic component of CLS09 is smoothed. The fact that this source of error does not appear in E^{η} tells us that this error is inherent in the MDT calculation rather than being intrinsic to the either the geoid or MSS fields.

Although the spectral method, by matching the spectral content of the MSS with that of the geoid, greatly reduces MDT error due to geoid truncation error, BHL14 will contain some noise due to imperfect spectral

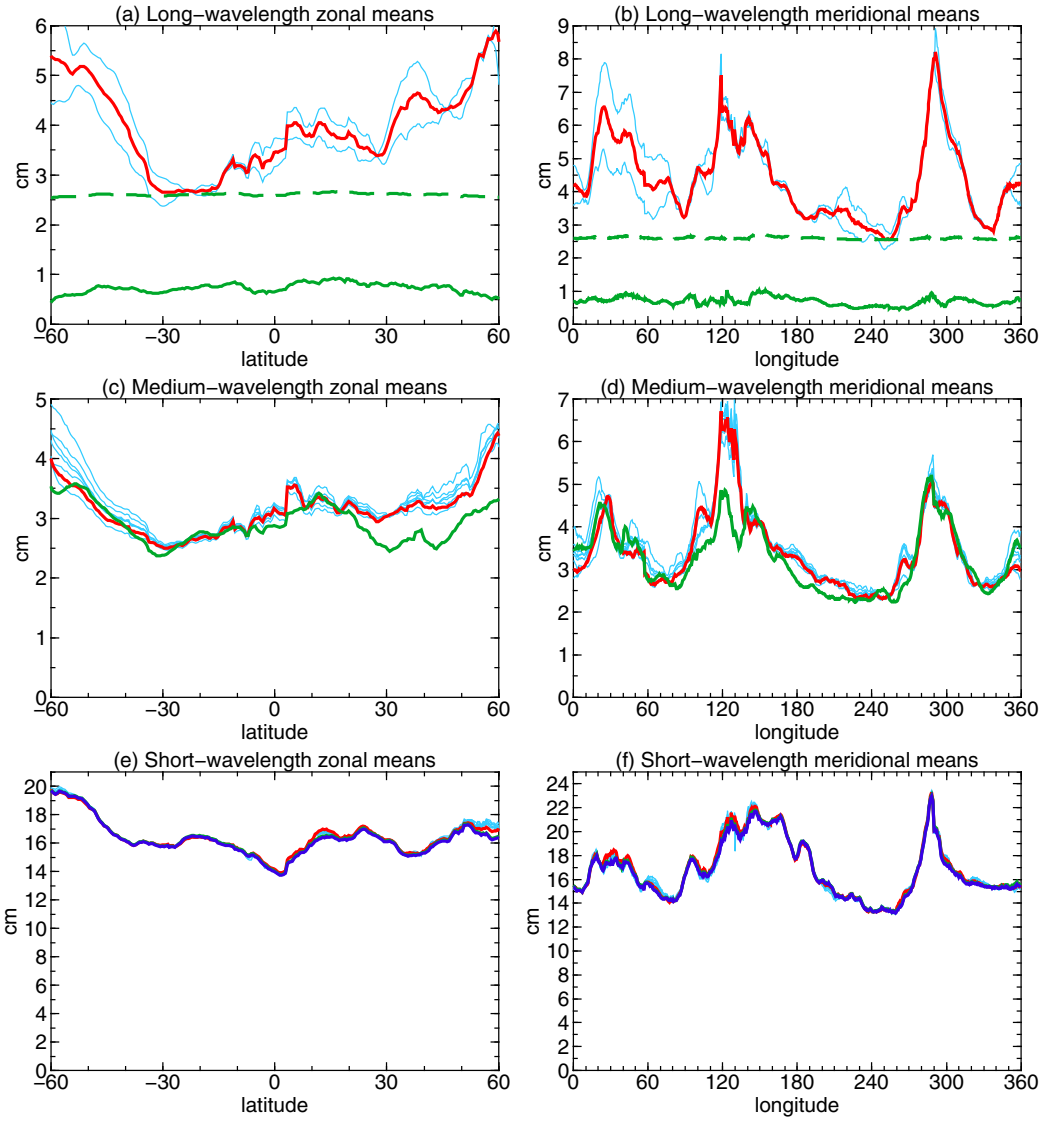

Figure 4. (a) Zonal means of the informal error estimates for the long-wavelength component of BHL14 with the following colours: best direct estimate (red), other direct estimates (cyan), quadratic sum of best CLS01 and GTIM3 errors (green), and the quadratic sum including numerical error due to imperfect spectral matching (green dashed). (b) Repeating Figure 4a for meridional mean errors. (c, d) As in Figures 4a and 4b but for the medium-wavelength errors. (e, f) Repeating Figures 4c and 4d for the short-wavelength errors. Also shown are the zonal and meridional means of the best informal GTIM3 error estimate (blue).

matching that will not be captured by the individual geoid and MSS error estimates which are based on comparisons between surfaces that have gone through identical spectral transformations. Imperfect matching occurs, in part, because the numerical integration of a gridded field, as is used to obtain a set of spectral coefficients for the MSS, is obviously not a direct analogue of the way in which the spectral coefficients of the gravity field are obtained. Imperfect matching also arises because of the difficultly in merging the MSS and geoid to produce a truly continuous global surface, which, when truncated, produces an error over the ocean that exactly cancels the truncation error of the geoid. Assuming this error to be uniformly distributed, with regional variations in ϵ^{η} due mainly to errors in the reference MDTs, our analysis allows us to estimate that this imperfect matching is associated with an error of roughly 2.5 cm, which when added quadratically to E^{η} gives the green dashed lines in Figures 4a and 4b. As such, this numerical error is the largest single source of error in the long-wavelength version of BHL14.

It is important to note, however, that just as increasing the maximum degree and order L at which the geoid is truncated reduces the error in an MDT calculated by the point-wise approach—that is, by simply

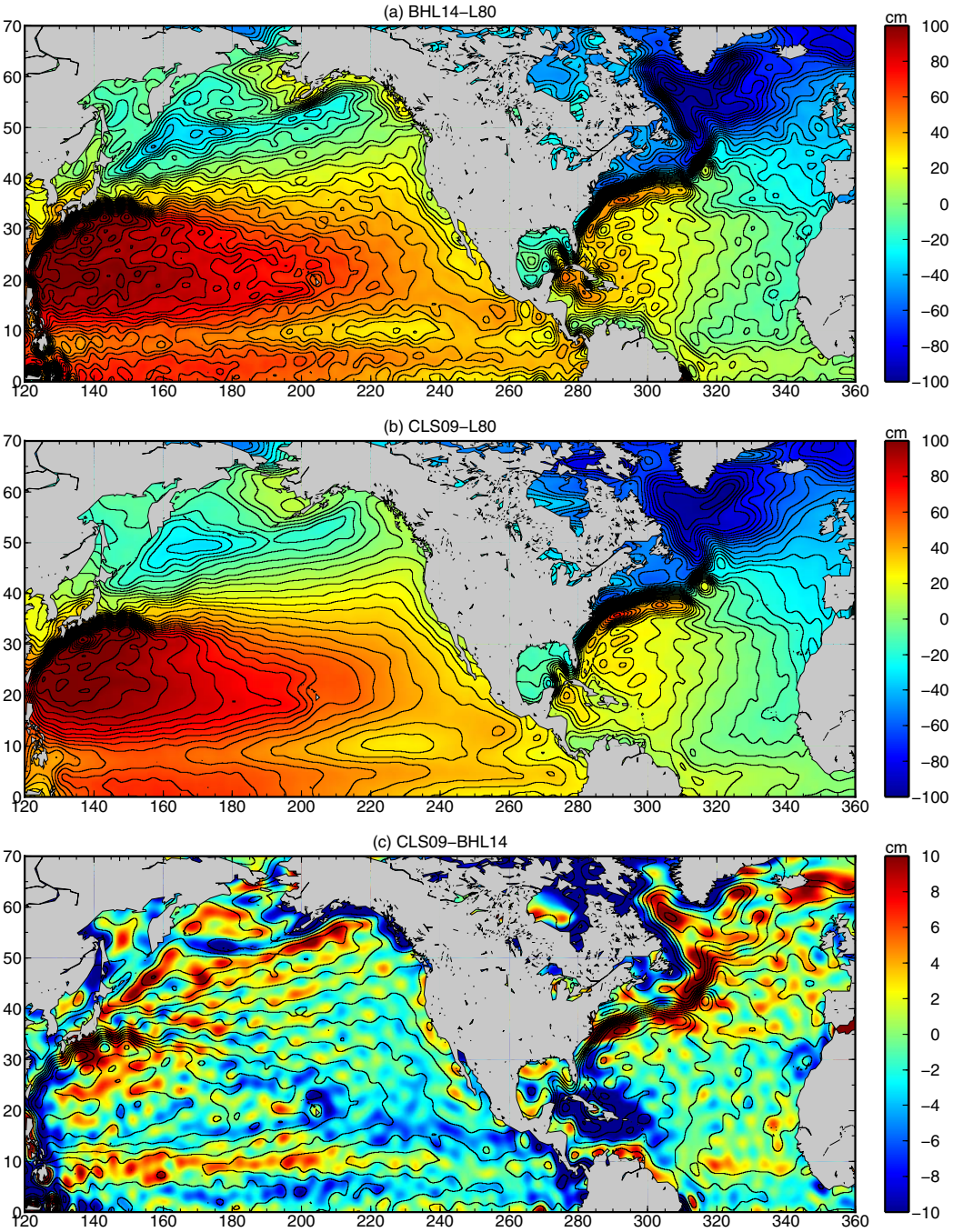

Figure 5. (a) The long-wavelength component of the BHL14 MDT with a contour interval of 5 cm. (b) Repeating Figure 5a for the CLS09 MDT. (c) The long-wavelength CLS09 MDT minus the long-wavelength BHL14 MDT, with contours from BHL14 with an interval of 10 cm.

subtracting a truncated geoid from a full MSS—the spectral MDT error due to imperfect spectral matching also diminishes with increasing L. At $L = 80$ the geoid truncation error in the point-wise version of BHL14 is 76 cm. Assuming that the numerical error in the spectral MDT remains a fixed fraction (3%) of the geoid truncation error, then for η_{150} this error is 1.4 cm and for η_{250} it is 1.0 cm, a negligible component of the total error. Therefore, we take the 1.7 cm error resulting from errors in GTIM3 and CLS01 as our best estimate of the *realized* error in the long-wavelength component of the full BHL14 MDT.

The best estimate of the MSS error is given by the CLS01/DTU10 RMS difference (Figure 6b) and has a global mean value of 1.3 cm. Figures 7a and 7b show that the set of informal GTIM3 errors are in close agreement,

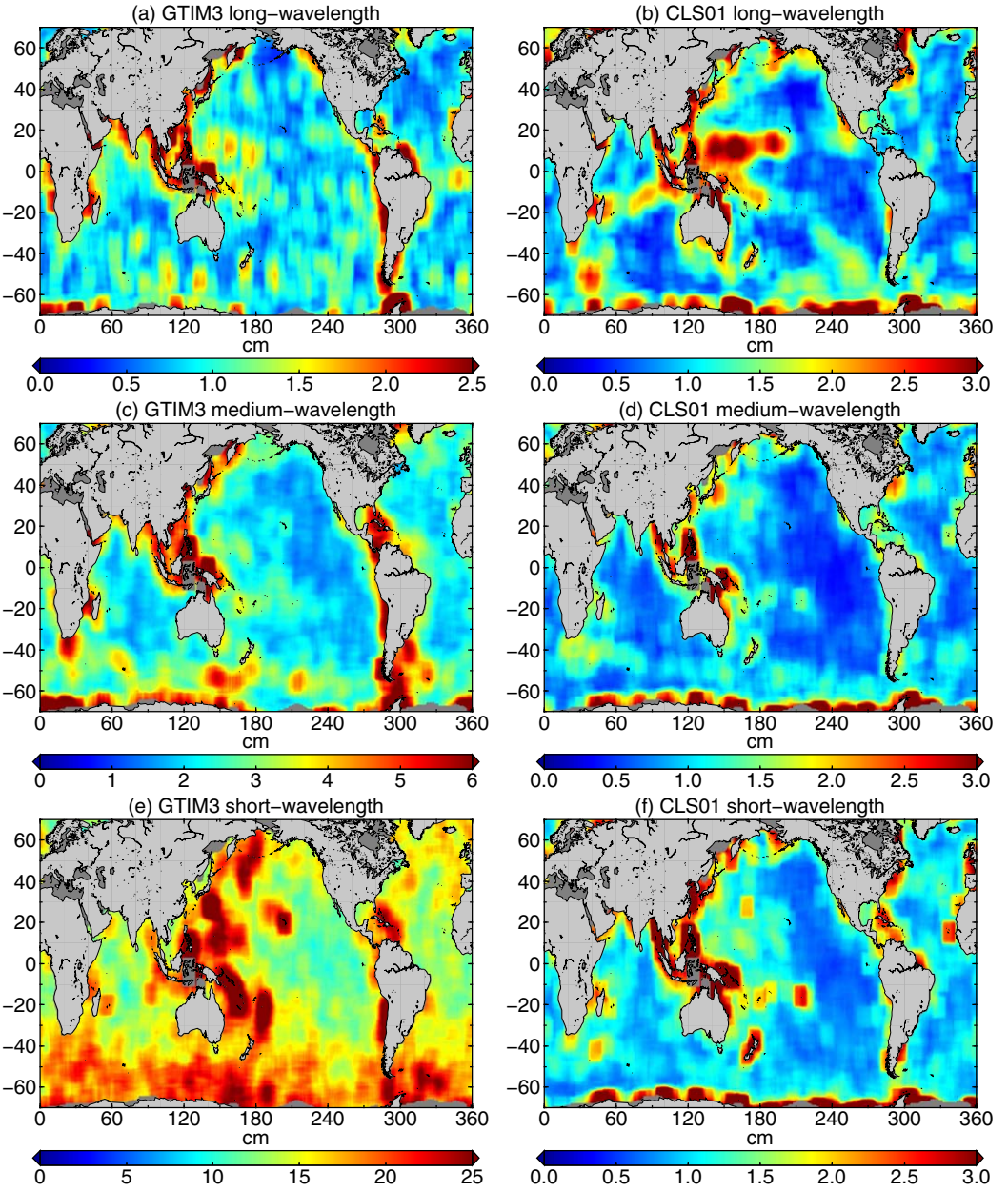

Figure 6. Informal error estimates for the long-wavelength components of (a) the GTIM3 geoid and (b) the CLS01 MSS. (c, d) Repeating Figures 6a and 6b for the medium-wavelength components of GTIM3 and CLS01. (e, f) Repeating Figures 6a and 6b for the short-wavelength components of GTIM3 and CLS01.

with the GTIM3/EGM2008 RMS difference (Figure 6a and red in Figures 7a and 7b), which has a global mean value of 1.1 cm, providing the best estimate of the GTIM3 error. The long-wavelength errors in the reference gravity models can be expected to be small compared with the GTIM3 error because the former include GRACE data, which is superior to GOCE data at long-wavelengths [*Pail et al.*, 2010b].

3.2. Medium-Wavelength Errors

Considering next the medium-wavelength component of BHL14, we find much better agreement between the direct ϵ^{η} and quadratic sum E^{η} error estimates (Figures 3d and 3e). For both, errors are greatest in the Southern Ocean, the Agulhas retroflection and Indonesian through-flow regions, the northwestern Pacific, and along the west and east coasts of America. Both error estimates have similar global mean values

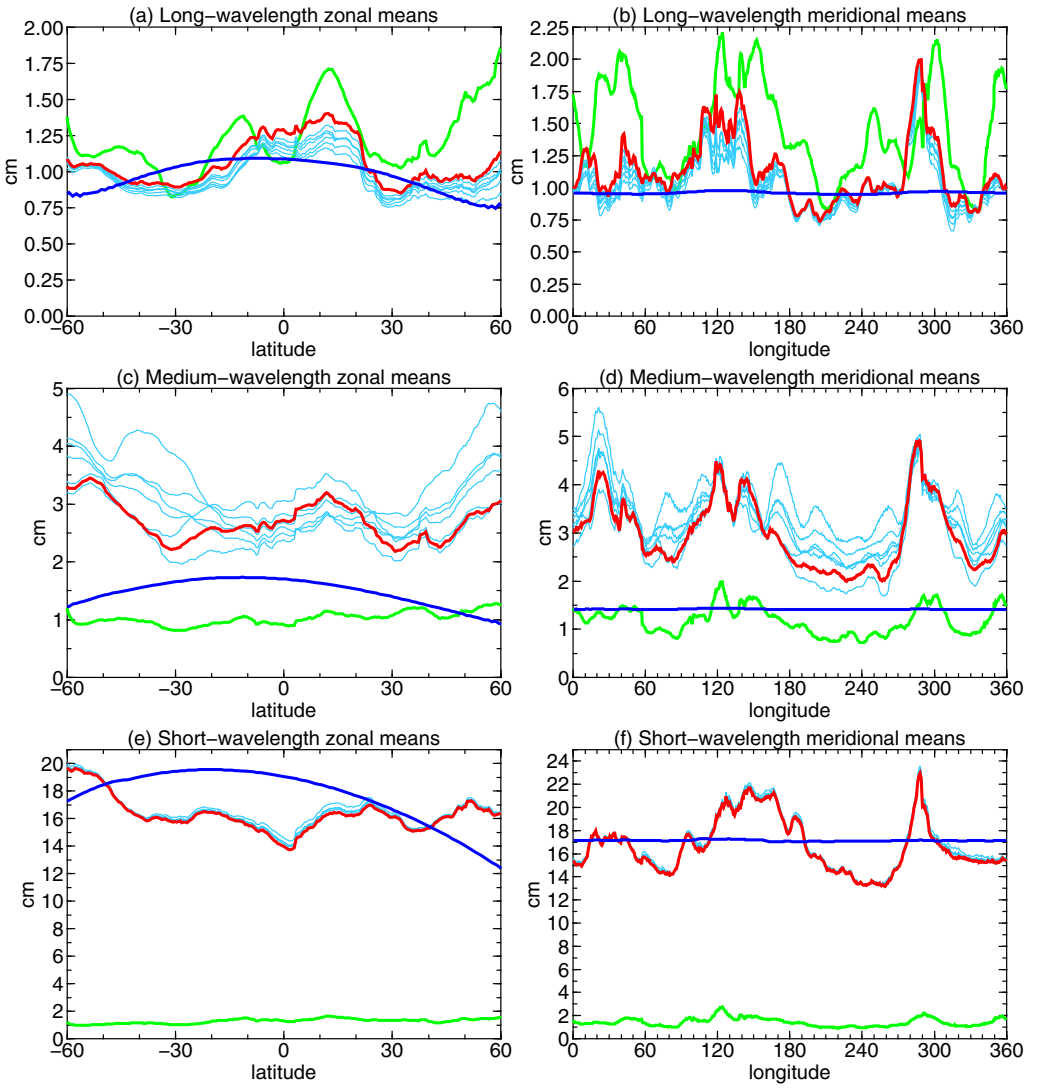

Figure 7. (a) Zonal means of the error estimates for the long-wavelength component of the GTIM3 geoid with the following colours: best informal estimate (red), the other informal estimates (cyan) and formal errors (blue). The best informal error for the CLS01 MSS is shown in green. (b) Repeating Figure 7a for meridional mean errors. (c, d) As in Figures 7a and 7b but for the medium-wavelength errors. (e, f) Repeating Figures 7a and 7b for the short-wavelength errors.

(3.1 cm for ϵ^{η} and 3.0 cm for E^{η}), and the zonal and meridional mean errors are in broad agreement (Figures 4c and 4d).

The geoid is now the largest contributor to the MDT error budget (Figures 7c and 7d). The best informal medium-wavelength GTIM3 error estimate, given by the mean of the EGM2008 and EIGEN51C-based RMS differences (Figure 6c and red in Figures 7c and 7d), has a global mean value of 2.8 cm. Meanwhile, the medium-wavelength CLS01 error estimate, given by the CLS01/DTU10 RMS difference (Figure 6d and red in Figures 8c and 8d) has a global mean value of 1.1 cm, similar in magnitude to the long-wavelength component.

The agreement between ϵ^{η} and E^{η} is not perfect, however. In terms of zonal means, ϵ^{η} and E^{η} disagree by about 0.5 cm just north of the equator, and ϵ^{η} diverges from E^{η} north of 15°N, eventually exceeding E^{η} by 1 cm at 60°N. The meridional mean agreement is generally better, accept near 120°N, where there is a peak of 7 cm in ϵ^{η} not found in E^{η}. As before, it is possible that ϵ^{η} may overestimate the true BHL14 error due to errors in the reference MDTs. In particular, the attenuation of the CLS09 and MAX11 gradients in regions of strong currents seen for the long-wavelength component may continue into the midwavelength band, meaning that medium-wavelength components of the CLS09 and MAX11 reference MDTs would be slightly

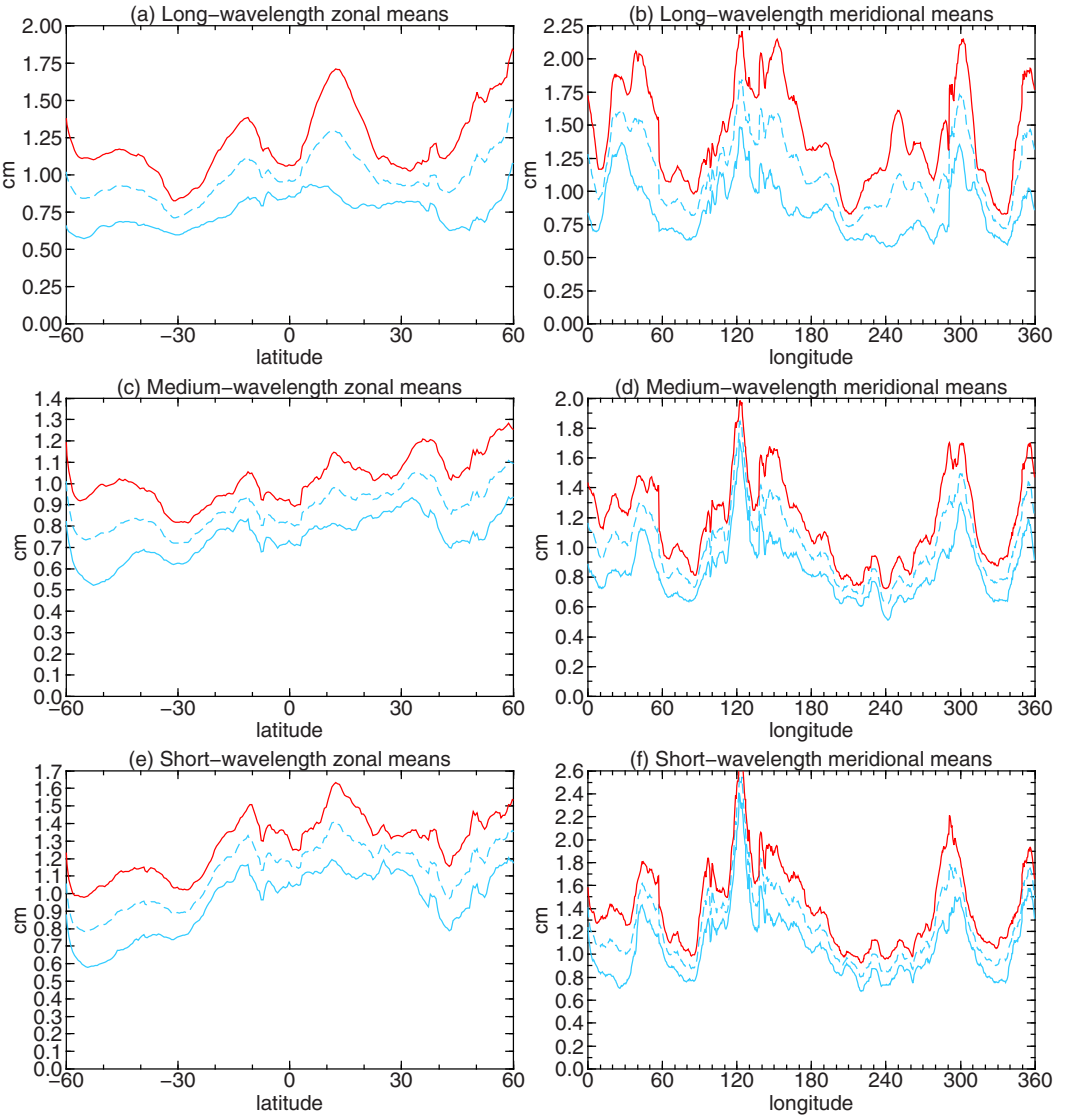

Figure 8. (a) Zonal means of the informal error estimates for the long-wavelength component of the CLS01 MSS with the following colours: the best estimate, given by the CLS01/DTU10 RMS difference (red), the CLS01/CLS11 RMS difference (cyan) and the mean CLS01/DTU10 and CLS01/CLS11 RMS differences (dashed cyan). (b) Repeating Figure 8a for meridional mean errors. (c, d) As in Figures 8a and 8b but for the medium-wavelength CLS01 errors. (e, f) Repeating Figures 8a and 8b for the short-wavelength CLS01 errors.

under-powered in regions of strong currents. This is confirmed in Figure 9 where find that in such regions the RMS amplitude of the medium-wavelength component of BHL14 (Figure 9a) is a little greater than the RMS amplitude of the medium-wavelength components of CLS09 (Figure 9c) and MAX11 (Figure 9d), with amplitudes closer to those of NLR03 (Figure 9b). This is noticeable in the subpolar gyre of the North Atlantic, along the boundary flowing path of the Gulf Stream, along the ACC, and in the Agulhas retroflection and the Brazil-Malvinas confluence regions. In this comparison we have removed the influence of the background noise on the BHL14 RMS amplitudes, by replacing the global mean RMS of BHL14 (3.7 cm) with that of NLR03 (2.3 cm).

There is also the additional error due to imperfect spectral matching as described earlier. This is particularly noticeable in the North Pacific and, together with the reference MDT error, leads to the Northern hemisphere difference between the zonal means in ϵ^{η} and E^{η}. Similarly, the peak in the meridional mean of ϵ^{η} near 120°E is due to imperfect spectral matching around the islands in the Indonesian through-flow region.

Regions where E^{η} is greater than ϵ^{η} require a different explanation. Just as is the case for ϵ^{η}, errors in the reference surfaces can lead to ϵ^{N} or ϵ^{H} overestimating the true error in GTIM3 or CLS01, meaning the quadratic

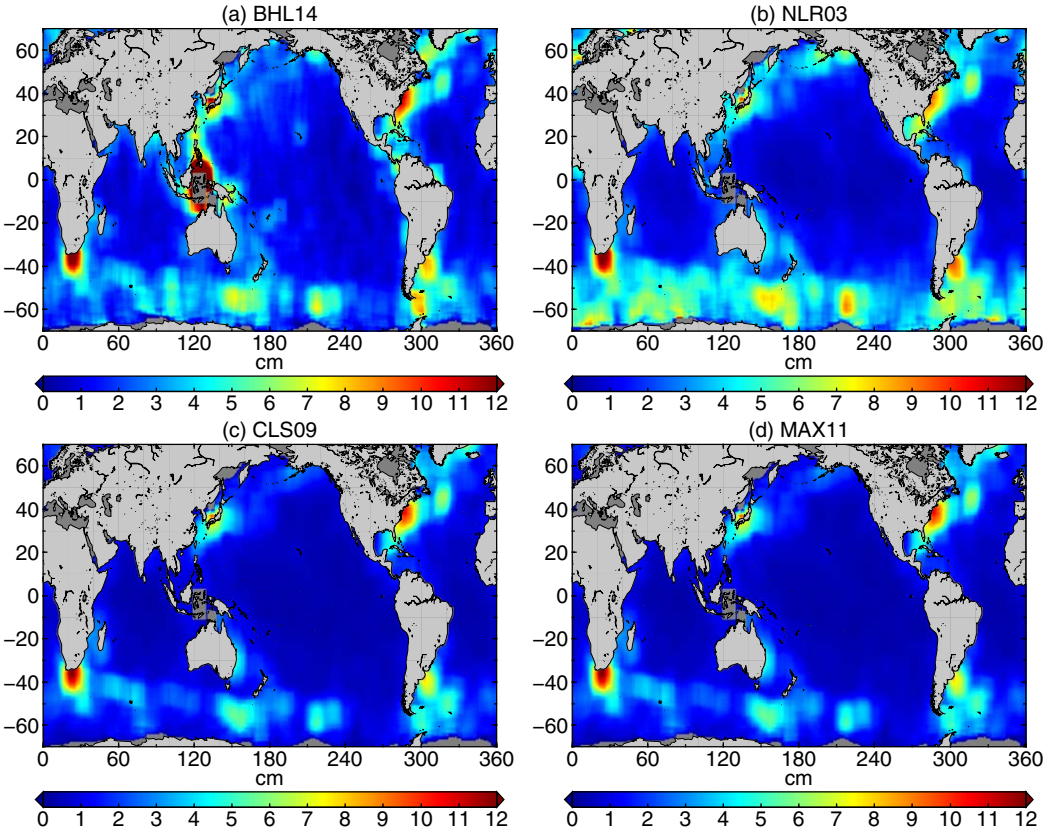

Figure 9. (a) The RMS amplitude of the medium-wavelength component of the BHL14 MDT, with the global mean RMS adjusted to that of the NLR03 MDT. (b-d) The RMS amplitude of the medium-wavelength component of the NLR03, CLS09 and MAX11 MDTs.

sum will also overestimate the actual BHL14 error. This is the case, for instance, on the eastern and western flanks of Africa extending south from 10° S (Figure 3f). We can infer from this, since GTIM3 is the dominant source of error in these regions, that GTIM3 is probably more accurate than EGM2008 and/or EIGEN51C in these regions. This is not surprising, since it is within this midrange of spatial scales that GOCE should improve the global gravity field, which is consistent with the fact that the informal GTIM3 error estimates have the greatest spread in the medium-wavelength band (Figures 7c and 7d, red and cyan).

3.3. Short-Wavelength Errors

Finally, we consider the short-wavelength component of BHL14 which is, in one sense, the most interesting because it includes the scales we must resolve if we are to improve the resolution of the geodetic method. If filtering is to be used to remove noise within this band, while retaining as much signal as possible, then an accurate estimate of the short-wavelength error (i.e., noise) is crucial.

The best short-wavelength error estimate ϵ^{η} is provided by the BHL14/CLS09 RMS difference (Figure 3g), although there is very little difference between the set of seven estimates (see Figures 4e and 4f, where the best estimate is shown in red and the other estimates are shown in cyan; in fact, they are so similar they are almost indistinguishable in these plots). The informal error estimate is effectively independent of the choice of reference MDT. Thus, we can be confident that ϵ^{η} is a good estimate of the error in the short-wavelength component of BHL14. This confidence is reinforced by the agreement between ϵ^{η} and E^{η} (Figure 3h and green in Figures 4e and 4f), with ϵ^{η} and E^{η} having global mean values of 16.5 and 16.4 cm, respectively. Only small local differences of up to 3 cm exist between the two error estimates (Figure 3i).

In Figures 3g and 3h there is a clear correspondence between steep sea floor topography and regions of elevated errors. In the Pacific, for example, errors are as low as 10 cm in much of the eastern Pacific where the sea floor is relatively smooth. In contrast, in the western Pacific, where many more island chains, sea mounts and ocean trenches are found, errors often exceed 25 cm. This correspondence is also clear along

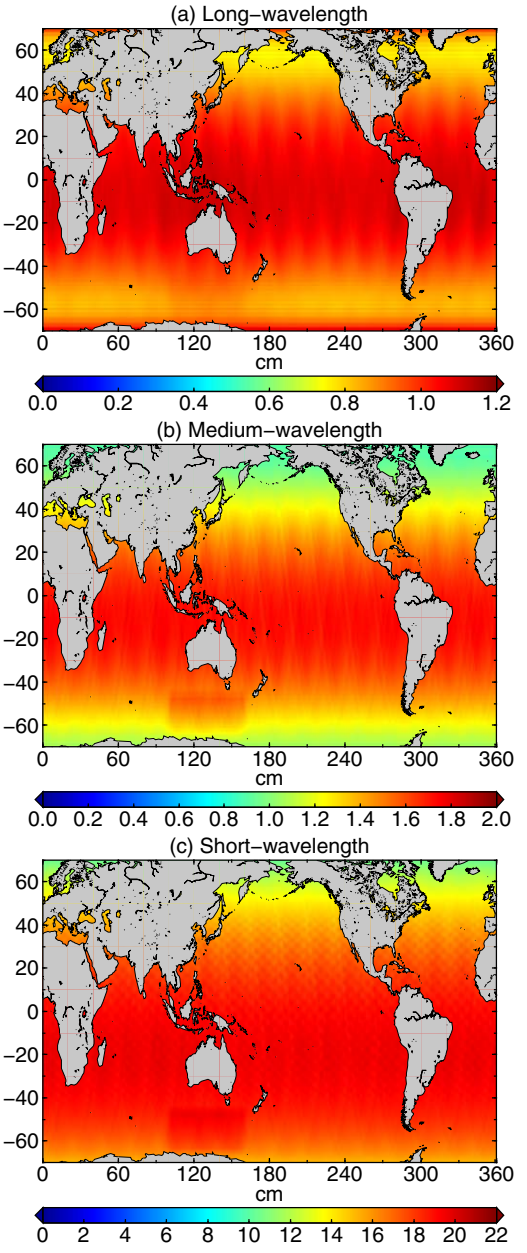

Figure 10. Formal errors for the (a) long, (b) medium, and (c) short-wavelength components of the GOCE GTIM3 geoid.

the Peru-Chile Trench in the southeastern Pacific and around the Caribbean islands in the North Atlantic. The Southern Ocean also stands out as a region of elevated errors, with short-wavelength errors exceeding 20 cm over much of its extent.

Comparing Figures 6e and 6f it is obvious that the GTIM3 geoid is largely responsible for the errors in the short-wavelength component of BHL14, a point reinforced by the close correspondence in Figures 4e and 4f between the informal short-wavelength errors for BHL14 (red) and GTIM3 (blue). In this case, ϵ^N is provided by the GTIM3/EIGEN51C RMS difference, although again there is little difference between the set of seven estimates (Figures 7e and 7f, where the best estimate is shown in red and the other estimates in cyan). As for BHL14, the informal GTIM3 error estimate is effectively independent of the choice of reference surface.

The short-wavelength CLS01 informal error estimates are in quite close agreement (Figures 8e and 8f). The CLS01/DTU10 RMS difference (red) provides the best informal error estimate for CLS01 and has a global mean value of 1.3 cm, negligible in comparison to the GTIM3 error (see Figures 7e and 7f).

4. Formal errors

Formal errors are also available for the GTIM3 geoid and the CLS01 MSS, and these serve as additional benchmarks for assessing the informal error estimates, and vice versa.

4.1. Formal Geoid Errors

Formal geoid errors are calculated from the full GTIM3 error variance-covariance matrix as described in Appendix B. Comparing the formal error maps for GTIM3 (Figure 10) with the corresponding informal errors for GTIM3 (Figures 6a, 6c, and 6e), the most obvious difference is that the formal errors show much less geographical variation than the RMS difference errors. The formal error magnitude decreases poleward, but shows little zonal variation. However, considering the zonal and meridional means of the long-wavelength error component (Figures 7a and 7b), we see that the formal error (blue) has a global mean of 1.0 cm, close to the 1.3 cm informal estimate (red). The short-wavelength error components (Figures 7e and 7f) also have similar global mean values of 16.4 cm for the informal estimate and 16.9 cm for the formal estimate. The zonal mean of the informal GTIM3 short-wavelength error does not show the same smooth dependence on latitude as the formal error, but does show the same hemispheric asymmetry, with errors greater in the southern hemisphere.

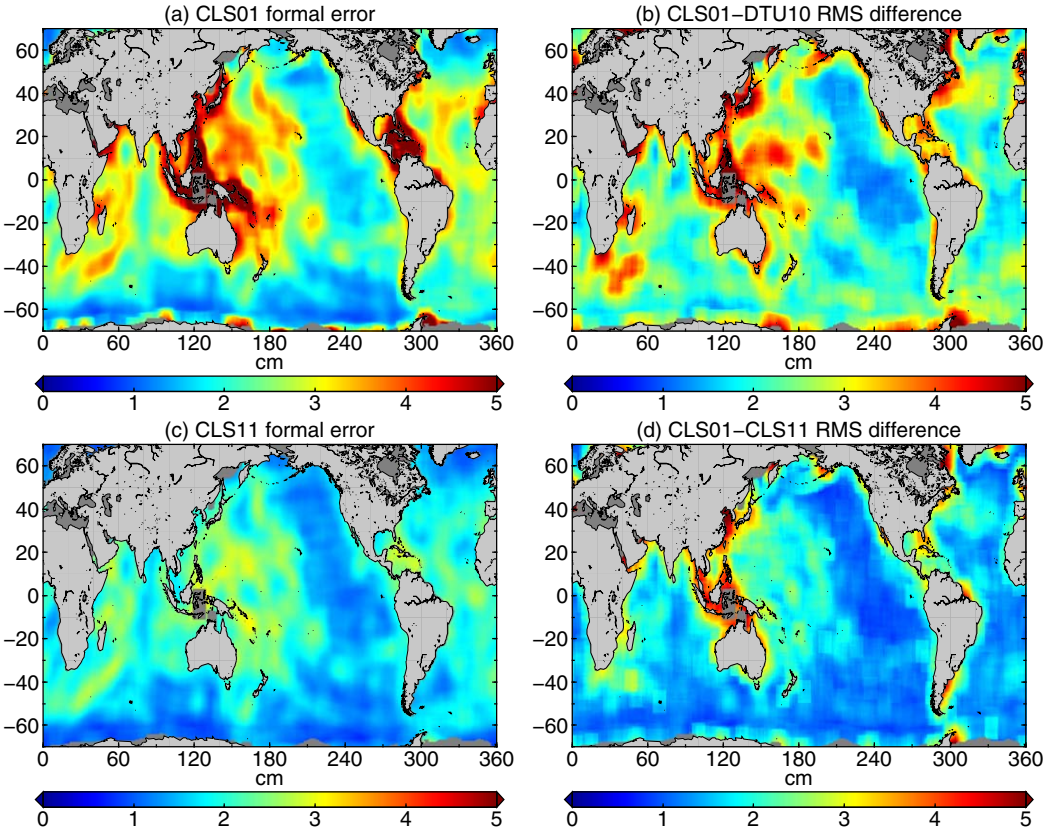

Figure 11. Formal errors for the (a) CLS01 MSS and (c) CLS11 MSS. The RMS difference between the MSS pairs: (b) CLS01 and DTU10; (d) CLS01 and CLS11.

The agreement is much worse for the medium-wavelength band (Figures 7c and 7d), where, with a mean value of 2.8 cm, the informal error is almost twice as large as the formal error (1.5 cm). Since it is in the medium-wavelength band that GOCE is expected to improve determination of the global gravity field, an initially plausible explanation for this discrepancy is that the informal errors overestimate the true medium-wavelength GTIM3 error because they reflect errors in the reference surfaces. However, while this might be the case if we were considering errors over land, over the ocean the reference surfaces include altimetric data. Given that the amplitude of the medium-wavelength MDT is small in comparison to the medium-wavelength geoid, the MSS will generally closely match the geoid and so, on average, over the ocean we can expect the combined gravity fields to be superior to GOCE and therefore the RMS differences to primarily reflect errors in the GOCE geoid. This analysis is supported by the agreement between ϵ^{η} and E^{η} within the medium-wavelength band, and suggests that the medium-wavelength formal error is too optimistic by a factor of two.

4.2. Formal MSS Errors

The CLS01 MSS is supplied with a formal error estimate arising from the optimal interpolation used to produce the MSS. To provide an error field of comparable spatial resolution to the informal error estimates, binning is used to reduce the resolution from the 2 minute grid to a 0.5 degree grid and then the mean error is computed in a $10^{\circ} \times 10^{\circ}$ window around each point (Figure 11a). Spatial variations of sea surface height due to the underlying sea floor topography is the primary geophysical factor governing the error magnitude. Errors tend to be greatest, rising to 4 cm, in regions, such as over the mid-Atlantic ridge and in the western Pacific, where steep sea floor topography produces correspondingly steep gradients in the sea surface.

Unfortunately, it is not possible to obtain formal MSS errors as a function of spatial scale as we can for the geoid. However, we can assess the RMS difference approach to estimating the CLS01 error by comparing the formal error with RMS differences calculated for the full mean sea surfaces—that is, without spectral

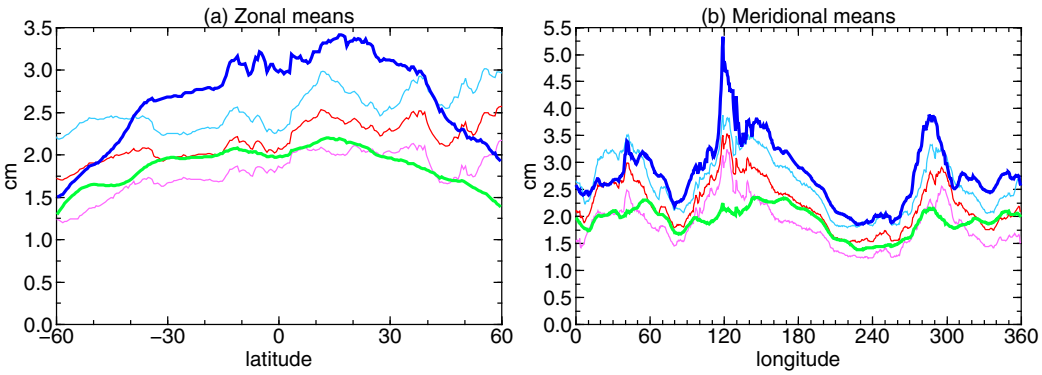

Figure 12. (a) Zonal means of the formal CLS01 error (blue), the formal CLS11 error (green) and informal CLS01 errors given by the CLS01/DTU10 RMS difference (light blue), the CLS0/CLS11 RMS difference (purple) and the mean of the CLS01/DTU10 and CLS01/CLS11 RMS differences (red). (b) As in Figure 12a but for the meridional mean errors.

truncation. The CLS01/DTU10 RMS difference (Figure 11b) provides the closest match to the formal CLS01 error. Global mean errors are 2.5 and 2.8 cm, respectively, and as can be seen from the meridional mean error plots (Figure 12b, where the formal error is shown in blue and the RMS difference in light blue), they are broadly similar in terms of the spatial variations in error magnitude. This agreement provides us with a degree of confidence that the CLS01/DTU10 RMS difference is a reasonable proxy for the CLS01 MSS error, and this is consistent with the fact that in the analysis above the CLS01/DTU10 RMS difference gave the best (most consistent) informal error estimate in each wavelength band.

Although from Figures 11a and 11b it would appear that the formal errors are too pessimistic in regions where topographic gradients are large, leading to the discrepancy between the zonal mean errors seen in Figure 12a, these values most likely reflect errors in the very small scales present in the full resolution MSS, but which are not relevant for the MDT calculation since they extend well below the scales that can be resolved in the geoid.

5. Improving the Geodetic MDT

So far we have focused on a particular geodetic MDT calculated using the CLS01 MSS and the GTIM3 geoid. This can be thought of as establishing a baseline against which improvements delivered by newer products can be assessed. In fact, the CLS11 MSS and GTIM4 geoid provide the most recent versions of the primary surfaces used in BHL14. Therefore, we now examine the impact that these surfaces have on the geodetic MDT calculation relative to BHL14.

At long-wavelengths (Figures 13a and 13b), the GTIM4 geoid reduces the global mean error by 1 mm, and the CLS11 MSS reduces it by a further 2 mm, giving a global mean error of 3.6 cm for the long-wavelength MDT. Remember, however, that this value also includes errors due to imperfect spectral matching and reference MDT errors. Based on the values obtained for BHL14, we estimate the global mean of this error to be $\sqrt{(\epsilon^{\eta})^2-(E^{\eta})^2}=3.5$ cm. Removing this from the global mean of ϵ^{η} for the GTIM4/CLS11 MDT, we obtain a final long-wavelength error of 0.8 cm, a factor of two improvement upon BHL14, with GTIM4 and CLS11 contributing 0.7 and 0.5 cm, respectively (where we have again assumed that all errors are independent and sum in quadrature). This is roughly in-line with the improvement from CLS01 to CLS11 implied by their formal errors (Figure 12).

For the medium-wavelength MDT component (Figures 13c and 13d) the more recent gravity field gives a reduction in the global mean error of 2 mm, while also using the more recent MSS product yields an additional 1 mm reduction in the global mean error, giving a final medium-wavelength error of 2.8 cm, with 2.6 cm coming from GTIM4 and 0.8 cm from CLS11.

The greatest improvement, resulting primarily from the newer gravity model, occurs for the short-wavelength component. Replacing GTIM3 with GTIM4 reduces the short-wavelength MDT error by 3.2 cm

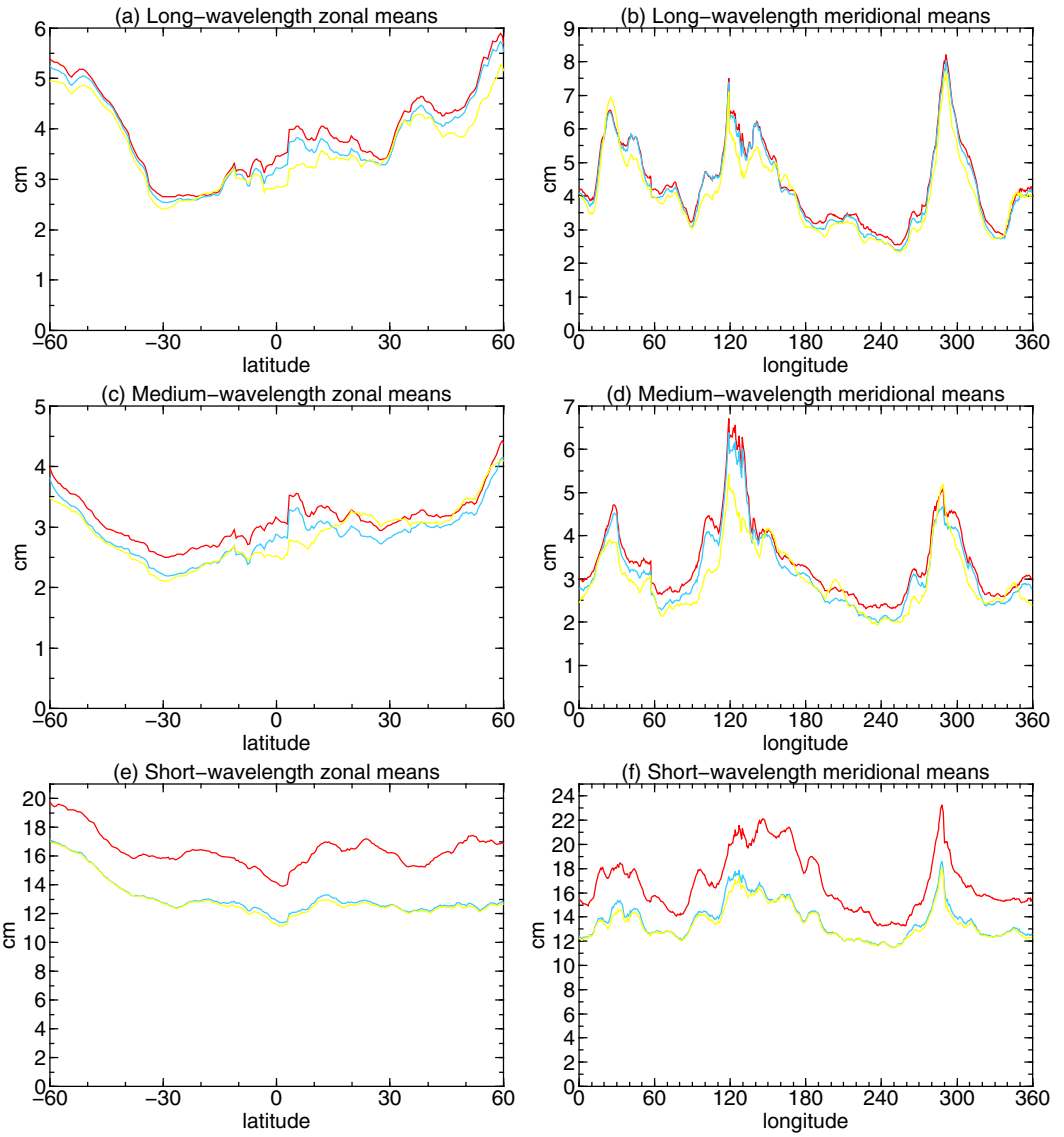

Figure 13. (a) Zonal means of the informal error estimates for the long-wavelength component of the CLS01/GTIM3 (BHL14; red), CLS01/GTIM4 (cyan) and CLS11/GTIM4 (yellow) geodetic mean dynamic topographies. (c, d) Repeating Figures 13a and 13b but for the medium-wavelength errors. (e, f) Repeating Figures 13c and 13d for the short-wavelength errors.

to 13.3 cm (Figures 13e and 13f). If we also use the more recent MSS we gain a further 2 mm error reduction. The much smaller impact of the more recent MSS is to be expected given the dominance of the geoid error contribution to the total short-wavelength error, and shows that gravity determination is still the limiting factor as far as improving the spatial resolution of the geodetic approach is concerned.

Table 1. Global Mean Error Estimates for the Three Wavelength Components of the BHL14 MDT and Its Constituent Surfaces, the GTIM3 Geoid and the CLS01 MSS

	η_{LW} (cm)	η_{MW} (cm)	η_{SW} (cm)
ϵ^{η}	3.9	3.1	16.5
E^{η}	1.7	3.0	16.4
ϵ^{N}	1.1	2.8	16.3
ϵ^{N}_{Formal}	1.0	1.5	16.9
ϵ^{H}	1.3	1.1	1.3

6. Concluding Discussion

The geodetic approach to estimating the ocean's mean dynamic topography offers a number of potential advantages over other approaches which rely on in situ data. However, careful consideration of the error characteristics of the geodetic approach is essential if these advantages are to be realized. This has been the primary motivation of the work

presented in this paper. To establish a baseline against which the impact of newer products can be assessed, we have initially focused on a geodetic MDT (BHL14) computed from the CLS01 MSS and a 3rd generation GOCE geoid (GTIM3).

Our analysis (summarized in Table 1) suggests that the long-wavelength component of the BHL14 MDT, corresponding to spatial scales greater than 250 km, has a global mean error of 1.7 cm, certainly a huge improvement on the 13 cm at 2000 km accuracy of an early geodetic MDT estimate reported by *Nerem et al*. [1990]. Within this band, the CLS01 MSS contributes 1.3 cm to the total error, slightly more than the 1.1 cm contributed by the GTIM3 geoid.

For the medium-wavelength component of our MDT, corresponding to spatial scales of 133–250 km, the global mean error is 3.0 cm. Combining the long and medium-wavelength error components quadratically we can infer that the version of BHL14 shown in Figure 1b, which is computed to $L = 150$, and so has a spatial resolution of approximately 133 km, has a global mean error of 3.4 cm. This is more than a factor of two improvement on the pre-GOCE MDT uncertainty of 10 cm at 170 km resolution found by *Vossepoel* [2007]. Within this band, the GTIM3 geoid is the dominant source of error, contributing 2.8 cm compared with a contribution of 1.1 cm from the CLS01 MSS.

If we wish to push the resolution of BHL14 to scales finer than 133 km, then we face the problem of rapidly growing geoid commission error. The short-wavelength component of BHL14 has a global mean error of 16.4 cm, more than four times the combined error in the long and medium-wavelength components. Within this range, compared to the 16.3 cm error in the GTIM3 geoid, the MSS makes a negligible contribution (1.3 cm) to the BHL14 error budget.

In this paper, we have derived informal errors for our geodetic MDT in two ways: The first, direct estimate is based on RMS differences between BHL14 and a range of independent MDTs, while the second estimate is obtained from the quadratic sum of analogous informal errors for the CLS01 MSS and the GTIM3 geoid. For the large-amplitude short-wavelength BHL14 errors, which are due almost entirely to errors in GTIM3, the two approaches give very similar error estimates, with the direct approach having a global mean value of 16.5 cm compared with 16.4 cm from the quadratic sum. Therefore, we can have immediate confidence that we have accurately estimated the short-wavelength error in BHL14, and, by extension, GTIM3.

As we move to longer wavelengths, however, the two approaches begin to diverge and so further interpretation is required to establish which of the two estimates is the more reliable. In the first instance, we should prefer the lower of the two error estimates since the RMS difference approach will tend to overestimate the true error because it will also reflect errors in the reference surfaces (assuming, of course, that the errors in the primary and reference surfaces are not positively correlated).

Taking the long-wavelength component as the extreme case, the BHL14 error estimate based on comparison with the reference MDTs gives a global mean error of 3.9 cm, compared with 1.7 cm obtained from the quadratic sum of MSS and geoid errors. Our analysis reveals that the direct approach overestimates the true long-wavelength BHL14 error for two reasons. First, the long-wavelength BHL14 MDT is contaminated with noise due to limitations of the spectral method, specifically imperfect spectral matching of the MSS and geoid. For applications using a low resolution MDT this error source should be taken into account. However, it diminishes as the maximum degree and order of the spectral MDT is increased, such that by the time we reach a truncation likely to be used in most applications (e.g., $L > 150$) it is a negligible source of error.

Errors in the reference MDTs is perhaps a more interesting reason why the direct and quadratic sum estimates diverge at long-wavelengths. In particular, the long-wavelength components of the CLS09 and MAX11 MDTs—formed by combining a smoothed GRACE-based geodetic MDT with in situ drifter and, for CLS09, hydrographic data—have weaker gradients than those of the long-wavelength component of BHL14. The relative weakness of the long-wavelength signal in the reference MDTs has a straightforward explanation: The CLS09 and MAX11 MDTs are based on a heavily smoothed geodetic estimate, which is then supplemented by in situ data to resolve the short spatial scales. However, it would seem that the in situ data does not restore the intermediate length scales that are lost when the geodetic MDT is filtered. This is also the case, but to a much lesser degree, with the medium-wavelength MDT components. So although the combined MDT products contain fine-scale features, these are superimposed on an attenuated long-wavelength background. This demonstrates the importance of carefully filtering the geodetic MDT to maximize the oceanographic

information that can be extract from it. (Note, this is not to say that BHL14 is superior to CLS09 or MAX11. BHL14 still contains noise that must be removed by filtering. The challenge remains to do this while preserving the signal that clearly exists in the unfiltered but noisy geodetic estimate.)

A limitation of the informal approach to estimating errors is the difficulty in finding a sufficiently large set of truly independent reference surfaces against which to assess our primary surfaces. This problem is most acute when trying to account for the CLS01 MSS contribution to the BHL14 error, especially when considering long wavelengths where CLS01 and GTIM3 appear to make similar contributions to the MDT error budget. The CLS01 error may be underestimated using the direct MDT-to-MDT comparisons in the case of CLS09 and MAX11 since these also use CLS01 to compute the initial geodetic MDT, and the errors in the MSS-free NLR03 MDT are too large to provide an independent assessment of the CLS09 and MAX11 based error estimates, as can be done for the medium and short-wavelength components. Likewise, the quadratic sum may underestimate the true error since CLS01 employs much the same data as the CLS11 and DTU10 surfaces and so systematic errors, such as those arising from the sea-state bias correction, may not be detected. Thus, we cannot rule out the possibility that the long-wavelength BHL14 error is somewhat underestimated due to an underestimation of the long-wavelength CLS01 error. However, given that there is no evidence for such a bias for the medium and short-wavelength components for which the MSS-free NLR03 estimate provides a truly independent estimate of the error, we may infer that any underestimation of the long-wavelength CLS01 error is likely to be small.

Formal errors are provided for the CLS01 MSS and the GTIM3 geoid. However, as recognized by *Wunsch and Gaposchkin* [1980], such errors cannot just be accepted as a true representation of actual error. The intercomparison of formal and informal error estimates, as we have attempt here, is one approach to assessing the reliability of both. The informal and formal GTIM3 errors have similar global mean values (see Table 1). However, while for the informal errors there is a clear relationship between the steepness of the sea floor topography and the magnitude of the error, the formal errors fail to capture this relationship.

While the supplied MSS formal error does not allow an analysis of the error magnitude as a function of spatial scale, it is still a useful benchmark for the informal MSS error. However, because the formal error is given as single field applicable to the full resolution MSS, which contains very small scales that contribute to the total error but which are not relevant to a geodetic MDT calculation, it should be considered an estimate of the upper bound on the MSS contribution to the geodetic MDT error. Indeed, it is the case that the formal CLS01 error is, with the exception of high latitudes, greater than the "best" informal estimate of the CLS01 error. The CLS01 formal error also confirms the finding of the informal analysis that the CLS01/DTU10 RMS difference gives this best informal estimate of the CLS01 error.

The short-wavelength component of BHL14 contains the scales we would like to resolve to improve the resolution of the geodetic method. Yet the magnitude of the errors in the short-wavelength component of BHL14 relative to the expected short-wavelength signal, as estimated from the three reference MDTs, which include in situ drifter data, make this challenging.

One approach to tackling this issue, and also the issue of long-wavelength signal attenuation seen in the combined products, is the gradient-preserving filtering method based on nonlinear diffusion [*Bingham*, 2010]. To control the severity to which the MDT is filtered, this method, in common with all spatial averaging filters, requires some measure of MDT noise. Some recent studies have employed heuristic strategies to estimate this noise [*Bingham et al*., 2011; *Knudsen et al*., 2011; *Siegismund*, 2013]. Our analysis shows that an informal approach to estimating geoid/MDT noise in this critical range of spatial scales is reasonable. This is fortunate given the relative ease by which the RMS difference metric can be computed.

However, while the diffusive filter takes into account the structure of the signal and the magnitude of the error (determined by the RMS difference approach), it cannot account for the error structure. Optimal filtering should incorporate knowledge of the magnitude and covariance structure of both the signal and the error. Because the geoid dominates the short-wavelength error, potentially the gravity model error variance-covariance matrix could be used to optimal filter the short-wavelength geodetic MDT component. Yet, as mentioned above, the formal GTIM3 error is too smooth and fails to capture the geographical variations in the true error and so this approach may fail. Assuming the error covariance structure of the geoid error is correct, this could possibly be resolved by combining the informal error magnitudes with the formal error covariances. However, more work is required to determine how this could be achieved.

Of course, the ideal solution is to improve the signal to noise ratio of the observations such that filtering is no longer necessary. In this study we have focused on a particular geodetic MDT calculated using the CLS01 MSS and GTIM3 geoid. This can be thought of as establishing a baseline against which the potential improvements delivered by newer products can be assessed. We find that the most recent GOCE gravity field product reduces the MDT error by 3 cm at scales finer than 133 km, and further reductions can be expected from subsequent releases. However, it seems likely that noise will remain and issue and filtering will still be required. In BHL14, it is only for scales greater than 250 km where the CLS01 MSS contributes about equally to the error and so it is at these length scales that improvements in the MSS should have the greatest impact. Indeed this is the case, with the CLS11 MSS reducing the long-wavelength geodetic MDT error by a factor of 2, in rough agreement with the improvement implied by the formal errors for the two surfaces. With this reduction in MSS error, the geoid becomes the dominant source of error for each wavelength component, and thus gravity field determination remains the limiting factor in geodetic MDT calculations.

Appendix A : Informal Error Estimation

A1. Method

Let $\phi_L \equiv \phi_L(\lambda,\theta)$ be the surface (geoid, MSS or MDT) for which we wish to derive an error estimate and ϕ'_L be an independent estimate of the same quantity, where L denotes the degree and order to which the surfaces have been expanded. When computed over a sufficiently large number of data points, the root mean square difference (denoted by $<*>$) between the primary surface and the reference surface can be written

$$\langle \phi_L - \phi'_L \rangle = \sqrt{(\epsilon^{\phi_L})^2 + (\epsilon^{\phi'_L})^2}, \tag{A1}$$

where ϵ^{ϕ_L} and $\epsilon^{\phi'_L}$ are the errors in the primary and reference surfaces respectively. When $\epsilon^{\phi'_L} \ll \epsilon^{\phi_L}$ this reduces to

$$\epsilon^{\phi_L} \approx \langle \phi_L - \phi'_L \rangle. \tag{A2}$$

and the RMS difference is a reasonable estimate of the error in ϕ_L. However, (A2) clearly cannot be true in general (otherwise there would be no need for estimate ϕ_L) and so the RMS difference metric must always be used with caution and where possible additional corroboration sought.

We must also consider what is meant by *a sufficiently large number of data points*. For each grid point the RMS difference is computed in a spatial window surrounding the point. Here we settled on a $10^\circ \times 10^\circ$. At midlatitudes the width of this window is approximately 800 km. Given that L corresponds to a spatial scale of approximately 20,000/L km, the number of degrees of freedom is $(L/25)^2$. Therefore, the robustness of (A1) is questionable for low truncations. In practice, however, the close correspondence between the formal and RMS difference geoid errors even at low truncations suggests the question of robustness is not an issue for our analysis.

A2. Reference Surfaces

A2.1. Gravity Models

For the purpose of assessing the formal geoid errors we employ three reference earth gravity models, all of which are based on a combination of satellite and terrestrial gravity data. Importantly, none use GOCE data. The models used are: (i) GIF48 is based on 66 months of GRACE data spanning the period 2003–2010 and the DTU10 terrestrial gravity data set, and is defined to degree and order 360 [*Ries et al.*, 2011]. (ii) EIGEN-51C is based on 6 years of CHAMP and GRACE data spanning the period 2002–2008, and the DNSC08 global gravity anomaly data set, and is defined to degree and order 359 [*Bruinsma et al.*, 2010]. (iii) Finally, EGM2008 is based on the ITG-GRACE03S global gravity model and a set of global gravity anomalies derived from terrestrial, altimetry-derived and airborne gravity data, and is defined to degree and order 2159 [*Pavlis et al.*, 2012].

A2.2. Mean Sea Surface Products

While CLS01 is supplied with a formal error field, for our analysis we also require an estimate of MSS error as a function of maximum degree and order L, information which is not readily available. As described below, this estimate will be based on a comparison with DTU10, which is computed from a combination of 17 years (1993–2009) of satellite altimetry from a total of 8 satellites [*Andersen and Knudsen*, 2009]. Gridded sea level anomalies from AVISO were used to adjust the MSS to the 1993–1999 period used in our analysis. Comparisons

were also made between CLS01 and CLS11, which is an updated version of CLS01, obtained using the same processing strategy but using 15 years of altimetry data (although still referenced to the 1993–1999 period).

A2.3. MDT Estimates

For the purpose of assessing the MDT error obtained by combining the geoid and MSS errors, we employ three reference MDTs: (i) The CLS09 MDT refers to the period 1993–1999. It uses in situ drifter and hydrographic data together with altimetric sea level anomaly data, and information from an MDT derived from an ocean model, to refine an initial geodetic MDT estimate based on a MSS and a GRACE geoid [*Rio et al*., 2011]. (ii) The Maximenko et al. MDT (MAX11 for brevity) is also a synthesis of a large-scale geodetic MDT, derived from a GRACE geoid and a MSS, and small-scale information provided by drifter, NCEP wind and altimetry data [*Maximenko et al*., 2009]. MAX11 covers the period 1992–2002 and the version used here is dated 7 January 2011. (iii) Finally, we use a 0.5° resolution MDT covering the period 1992–2003 calculated by *Niiler et al*. [2003] (which we denote NLR03 in the text). A distinguishing feature of this MDT is that it is not based on gravity data. Rather, it is derived from altimetry and in situ drifter data corrected for nongeostrophic motions, including Ekman transport and inertial motion.

While the native spherical harmonic representation of EGMs naturally requires the geoid to be specified to a maximum degree and order *L*, this is not generally the case for MSS or MDT products. Therefore, to compute an informal error for either of these surfaces requires that we compute their spherical harmonic representation, from which their truncated grid form can be determined to a given *L*. If ϕ' rather than ϕ'_L were used in the equation (A1), then the informal error estimate would include an omission error component, which would dominate the error estimate for low *L*. For the MSS, the spherical harmonic form is computed as it is for the MDT calculation, with a geoid filling land and other undefined regions [see *Bingham et al*., 2008]. For the reference MDTs, land and undefined regions are filled by linear interpolation before the spherical harmonic coefficients are calculated to reduce the Gibbs fringe effects due to the discontinuities at land/undefined boundaries.

Appendix B : Formal Geoid Errors

Also provided to the user community by the GOCE High-level Processing Facility are the full error variance-covariance matrices for each gravity model (*Pail et al*. [2011]; obtained from http://eo-virtual-archive1.esa.int/). Ultimately, we are interested in how these formal errors are expressed in the MDT. To achieve this, we must express the gravity field errors in terms of geoid error. We do this using the error propagation tools developed by *Balmino* [2009], which can be obtained from https://earth.esa.int/web/guest/software-tools.

The theoretical description of the error propagation performed by the Balmino routine covhsmp to obtain the geoid error field is as follows: Let the gridded geoid be given by

$$N(\lambda,\theta)=\overrightarrow{Y}^{T}X, \tag{B1}$$

where λ is longitude and θ is geocentric latitude and

$$\overrightarrow{X}=\{C_{lm};S_{lm}\} \tag{B2}$$

are the spherical harmonic coefficients of degree *l* and order *m* of the earth gravity model (in this case GTIM3), and

$$\overrightarrow{Y}=\{f_{lm}P_{lm}(\sin\theta)\cos m\lambda;f_{lm}P_{lm}(\sin\theta)\sin m\lambda\} \tag{B3}$$

are the standard spherical harmonic functions with

$$f_{lm}=\frac{GM}{r\gamma}\left(\frac{R}{r}\right)^{l}, \tag{B4}$$

where *GM* is earth's gravitational mass constant, *R* is earth's mean radius, γ is normal gravity at the computation point and *r* is radial distance. Then the corresponding geoid error field is given by:

$$\epsilon^{N}_{formal}(\lambda,\theta)=\sqrt{\overrightarrow{Y}^{T}\overrightarrow{\Gamma}\overrightarrow{Y}}, \tag{B5}$$

where $\overrightarrow{\Gamma}$ is the error variance-covariance matrix for GTIM3, with ordering consistent with $\overrightarrow{Y}$.

Formal geoid errors for the GTIM3 gravity model were computed from the error variance-covariance matrix for geoids with truncations $L=10$ to 250 in 10 degree intervals.

Acknowledgments
R.J. Bingham was supported by a fellowship from the UK National Centre for Earth Observation and by the ESA's GOCE User Toolbox (GUT) project. We would like to thank three anonymous reviewers for their valuable comments and suggestions which helped us greatly improve the original manuscript.

References

Andersen, O., and P. Knudsen (2009), DNSC08 mean sea surface and mean dynamic topography models, *J. Geophys. Res.*, *114*, C11001, doi:10.1029/2008JC005179.

Balmino, G. (2009), Efficient propagation of error covariance matrices of gravitational models: Application to GRACE and GOCE, *J. Geod.*, *83*, 989–995.

Bingham, R., K. Haines, and C. Hughes (2008), Calculating the ocean's mean dynamic topography from a mean sea surface and a geoid, *J. Atmos. Oceanic Technol.*, *25*(10), 1808–1822, doi:10.1175/2008JTECHO568.1.

Bingham, R. J. (2010), Nonlinear anisotropic diffusive filtering applied to the ocean's mean dynamic topography, *Remote Sens. Lett.*, *1*(4), 205–212, doi:10.1080/01431161003743165.

Bingham, R. J., P. Knudsen, O. Andersen, and R. Pail (2011), An initial estimate of the North Atlantic steady-state geostrophic circulation from GOCE, *Geophys. Res. Lett.*, *38*, L01606, doi:10.1029/2010GL045633.

Bruinsma, S., J. Marty, G. Balmino, R. Biancale, C. Foerste, O. Abrikosov, and H. Neumayer (2010), Goce gravity field recovery by means of the direct numerical method, paper presented at the ESA Living Planet Symposium, Bergen, Norway, 28 Jun-2 Jul.

Denker, H., and R. H. Rapp (1990), Geodetic and oceanographic results from the analysis of 1 year of Geosat data, *J. Geophys. Res.*, *95*(C8), 13,151–13,168, doi:10.1029/JC095iC08p13151.

Drecourt, J.-P., K. Haines, and M. Martin (2006), Influence of systematic error correction on the temporal behavior of an ocean model, *J. Geophys. Res.*, *111*, C11020, doi:10.1029/2006JC003513.

Featherstone, W. E., and M. Filmer (2012), The north-south tilt in the Australian Height Datum is explained by the ocean's mean dynamic topography, *J. Geophys. Res.*, *117*, C08035, doi:10.1029/2012JC007974.

Haines, K., D. Lea, and R. Bingham (2011), Using the GOCE MDT in ocean data assimilation, paper presented at 4th International GOCE User Workshop, Munich, Germany, 31 Mar-1 Apr.

Hernandez, F., and P. Schaeffer (2001), The CLS01 Mean Sea Surface: A validation with the GSFC00.1 surface, technical report, 14 pp., CLS, Ramonville St Agne, France.

Jayne, S., J. Wahr, and F. Bryan (2003), Observing ocean heat content using satellite gravity and altimetry, *J. Geophys. Res.*, *108*(C2), 3031, doi:10.1029/2002JC001619.

Knudsen, P., R. Bingham, O. Andersen, and M.-H. Rio (2011), A global mean dynamic topography and ocean circulation estimation using a preliminary GOCE gravity model, *J. Geod.*, *85*(11), 861–879.

Lea, D. J., J.-P. Drecourt, K. Haines, and M. J. Martin (2008), Ocean altimeter assimilation with observational- and model-bias correction, *Q. J. R. Meteorol. Soc.*, *134*(636), 1761–1774, doi:10.1002/qj.320.

Maximenko, N., P. Niiler, M.-H. Rio, O. Melnichenko, L. Centurioni, D. Chambers, V. Zlotnicki, and B. Galperin (2009), Mean dynamic topography of the ocean derived from satellite and drifting buoy data using three different techniques, *J. Atmos. Oceanic Technol.*, *26*(9), 1910–1919, doi:10.1175/2009JTECHO672.1.

Nerem, R. S., B. D. Tapley, and C. K. Shum (1990), Determination of the ocean circulation using Geosat altimetry, *J. Geophys. Res.*, *95*(C3), 3163–3179, doi:10.1029/JC095iC03p03163.

Niiler, P., N. Maximenko, and J. McWilliams (2003), Dynamically balanced absolute sea level of the global ocean derived from near-surface velocity observations, *Geophys. Res. Lett.*, *30*(22), 2164, doi:10.1029/2003GL018628.

Pail, R., H. Goiginger, R. Mayrhofer, W.-D. Schuh, J. Brockmann, I. Krasbutter, E. Hock, and T. Fecher (2010a), Goce gravity field model derived from orbit and gradiometry data applying the time-wise method, paper presented at ESA Living Planet Symposium, Eur. Space Agency, Bergen, Norway.

Pail, R., et al. (2010b), Combined satellite gravity field model GOCO01S derived from GOCE and GRACE, *Geophys. Res. Lett.*, *37*, L20314, doi:10.1029/2010GL044906.

Pail, R., et al. (2011), First GOCE gravity field models derived by three different approaches, *J. Geod.*, *85*, 819–843, doi:10.1007/s00190-011-0467-x.

Pavlis, N., S. Holmes, S. Kenyon, and J. Factor (2012), The development and evaluation of the Earth Gravitational Model 2008 (EGM2008), *J. Geophys. Res.*, *117*, B04406, doi:10.1029/2011JB008916.

Ries, J., S. Bettadpur, S. Poole, and T. Richter (2011), Mean background gravity fields for grace processing, paper presented at GRACE Science Team Meeting, Austin, Tex., 8–10 Aug.

Rio, M. H., S. Guinehut, and G. Larnicol (2011), New CNES-CLS09 global mean dynamic topography computed from the combination of grace data, altimetry, and in situ measurements, *J. Geophys. Res.*, *116*, C07018, doi:10.1029/2010JC006505.

Schaeffer, P., Y. Faugre, J. F. Legeais, A. Ollivier, T. Guinle, and N. Picot (2012), The CNES-CLS11 global mean sea surface computed from 16 years of satellite altimeter data, *Mar. Geod.*, *35*(S1), 3–19, doi:10.1080/01490419.2012.718231.

Siegismund, F. (2013), Assessment of optimally filtered recent geodetic mean dynamic topographies, *J. Geophys. Res.*, *118*, 108–117, doi:10.1029/2012JC008149.

Tai, C. K., and C. Wunsch (1983), Absolute measurement by satellite altimetry of dynamic topography of the Pacific Ocean, *Nature*, *301*(5899), 408–410, doi:10.1038/301408a0.

Tapley, B., D. Chambers, S. Bettadpur, and J. Ries (2003), Large scale ocean circulation from the GRACE GGM01 geoid, *Geophys. Res. Lett.*, *30*(22), 2163, doi:10.1029/2003GL018622.

Volkov, D. L., and V. Zlotnicki (2012), Performance of GOCE and GRACE-derived mean dynamic topographies in resolving Antarctic Circumpolar Current fronts, *Ocean Dyn.*, *62*(6), 893–905, doi:10.1007/s10236-012-0541-9.

Vossepoel, F. C. (2007), Uncertainties in the mean ocean dynamic topography before the launch of the Gravity field and steady-state Ocean Circulation Explorer (GOCE), *J. Geophys. Res.*, *112*, C05010, doi:10.1029/2006JC003891.

Woodworth, P., C. Hughes, R. Bingham, and T. Gruber (2013), Towards worldwide height system unification using ocean information, *J. Geod. Sci.*, *2*(4), 302–318, doi:10.2478/v10156-012-0004–8.

Wunsch, C., and E. M. Gaposchkin (1980), On using satellite altimetry to determine the general circulation of the oceans with application to geoid improvement, *Rev. Geophys.*, *18*(4), 725–745, doi:10.1029/RG018i004p00725.